Current Research in Microbial Sciences 10 (2026) 100613

Contents lists available at ScienceDirect

Current Research in Microbial Sciences

journal homepage: www.sciencedirect.com/journal/current-research-in-microbial-sciences

Integrated omics reveal a unique antibacterial mechanism of action for the small molecule HSI#6

Haitham Sedky [a,b], Mohamed Belal Hamed [a,c], Kurt Vermeire [a], Joost Schymkowitz [d], Spyridoula Karamanou [a,*], Anastassios Economou [a,1]

[a] Department of Microbiology, Immunology and Transplantation, Rega Institute, KULeuven, Herestraat 49, 3000 Leuven, Belgium
[b] Department of Microbiology and Immunology, Faculty of Pharmacy, Assiut University, Egypt
[c] Molecular Biology Department, National Research Centre, Cairo, Egypt
[d] Switch Laboratory, VIB Center for Brain and Disease Research and Department of Cellular and Molecular Medicine, Herestraat 49, 3000 Leuven, Belgium

ARTICLE INFO

Keywords:
Antibacterial
Omics
Small molecule
Envelope stress

ABSTRACT

The continuous risk of antibiotic resistance development underscores the demand for new agents with mechanisms distinct from existing antibacterial drugs. Here, we investigated HSI#6, a small-molecule antibacterial previously identified as a SecA activator, using integrated omics and functional assays. HSI#6 exhibits a rapid, broad-spectrum bacteriostatic activity, and induces a distinct cell envelope-homeostasis stress signature accompanied by global stress reprogramming. Time-resolved transcriptomics and proteomics revealed early activation of envelope stress regulons and oxidative stress pathways, followed by suppression of ribosome biogenesis and central metabolism. Comparative analysis and biomarker-based principal component analysis (PCA) positioned HSI#6 within the envelope stress mechanistic space, closely aligned with membrane-active antibiotics yet displaying a distinct signature. Adaptive laboratory evolution (ALE) combined with whole-genome sequencing (WGS) revealed compensatory mutations in topoisomerase 1A gene (*topA*) and transcriptional regulators, without adaptive resistance emerged even under prolonged selection pressure. These findings establish HSI#6 as a mechanistically unique antibacterial agent with low resistance potential.

Introduction

Antibiotic resistance is a critical global health challenge, eroding the effectiveness of existing therapies and driving an urgent need for new antimicrobials with novel mechanisms of action to minimize cross-resistance (Butler, Vollmer et al. 2024; Piddock, Malpani et al. 2024). Unlike most pharmaceuticals, antibiotics face persistent selective pressure, leaving bacteria with two options: death or survival by developing resistance, and pathogens have consistently evolved resistance to all conventional antibiotic classes (Miller and Arias 2024; Shah, Bhat et al. 2024). Current antibiotics primarily target cell wall biogenesis, DNA replication and protein synthesis, yet these pathways have been extensively exploited and circumvented by variable resistance mechanisms (Abushaheen, Muzaheed et al. 2020, Elbaiomy, El-Sappah et al. 2025, Zhang et al. 2022). Combination therapies offer temporary solutions for infections such as tuberculosis, *Acinetobacter baumannii* and Helicobacter pylori however, predicting synergistic interactions among antibiotics remains challenging (Bollenbach, Quan et al. 2009; Larkins-Ford and Aldridge 2023) (Yousfi, el-Zimaity et al. 1995; Larkins-Ford, Degefu et al. 2022; Morales-Durán, León-Buitimea et al. 2024; Rubio, zur Nedden et al. 2026; Tang, Sánchez-Hevia et al. 2024).

Integrated omics approaches have transformed the characterization of antibiotic mechanisms of action, enabling system-level interrogation of bacterial responses to antimicrobial stress (Pulido, García-Quintanilla et al. 2016; Warrier, Romano et al. 2022). Whole-genome sequencing of drug-exposed or evolved populations identifies resistance-conferring mutations, delineates evolutionary trajectories under selection pressure, and reveals essential genes and compensatory pathways that govern tolerance (Ma, Xu et al. 2025; Sherry, Lee et al. 2025). Transcriptomics complement this by capturing induced changes in gene expression, revealing early stress responses, regulatory network rewiring, and pathway-specific signatures that correlate with the antibiotic

* Corresponding author.
E-mail addresses: haitham.abdallah@kuleuven.be (H. Sedky), mohamed.soliman@kuleuven.be (M.B. Hamed), kurt.vermeire@kuleuven.be (K. Vermeire), joost.schymkowitz@kuleuven.be (J. Schymkowitz), lily.karamanou@kuleuven.be (S. Karamanou), aeconomo@me.com (A. Economou).
[1] Deceased.

https://doi.org/10.1016/j.crmicr.2026.100613

Available online 23 May 2026

mechanism of action (Domínguez, Muñoz et al. 2017; French, Guo et al. 2024; Poonawala, Zhang et al. 2024). These transcriptional fingerprints can classify new compounds into mechanistic categories and identify cognate targets within hours of exposure, substantially accelerating both mechanistic classification and antibiotic discovery (Bie, Zhang et al. 2023; Espinoza, Dupont et al. 2021). Proteomics extend this picture to the functional level, resolving the activation of envelope stress sensors, efflux systems, and metabolic remodeling that ultimately determine bacterial fate under drug exposure (Aita, Ristori et al. 2025; Senges, Stepanek et al. 2020; Torres-Sangiao, Giddey et al. 2022; Yu, O'Rourke et al. 2020). Time-resolved multi-omics workflows further reconstruct the temporal sequence of cellular events, from initial drug-target engagement to downstream stress reprogramming, providing mechanistic resolution that no single platform can achieve alone (Wecke and Mascher 2011). The integration of these orthogonal datasets clarifies complex modes of action, uncovers robust biomarkers of antibiotic class and target engagement, and informs on rational drug design (Morabito, De Simone et al. 2025; Wecke and Mascher 2011). Collectively, this shift from single-target interrogation to system-level profiling offers powerful new strategies for understanding and countering antimicrobial resistance.

Membrane targeting antibiotics stand out as an efficient class. They break membrane integrity, ion gradients, and energy balance, skipping the inhibition of usual biosynthetic paths which makes them less susceptible to resistance development. Transcriptomic studies of agents such as polymyxins, ionophores (e.g., monactin, valinomycin), and lipopeptides reveal early induction of envelope stress regulons (Cpx, Rcs, σ^E), activation of two-component systems and upregulation of efflux pumps, reflecting attempts to restore membrane stability under stress (Bie, Zhang et al. 2023; O'Rourke, Beyhan et al. 2020; Zhao, Wu et al. 2023). Proteomic studies corroborate these findings, showing enrichment of ABC transporters, chaperones and stress-response proteins alongside suppression of oxidative phosphorylation and ribosome biogenesis (Torres-Sangiao, Giddey et al. 2022). These omics signatures distinguish membrane-active agents from inhibitors of protein or fatty acid synthesis and serve as robust biomarkers for mechanistic

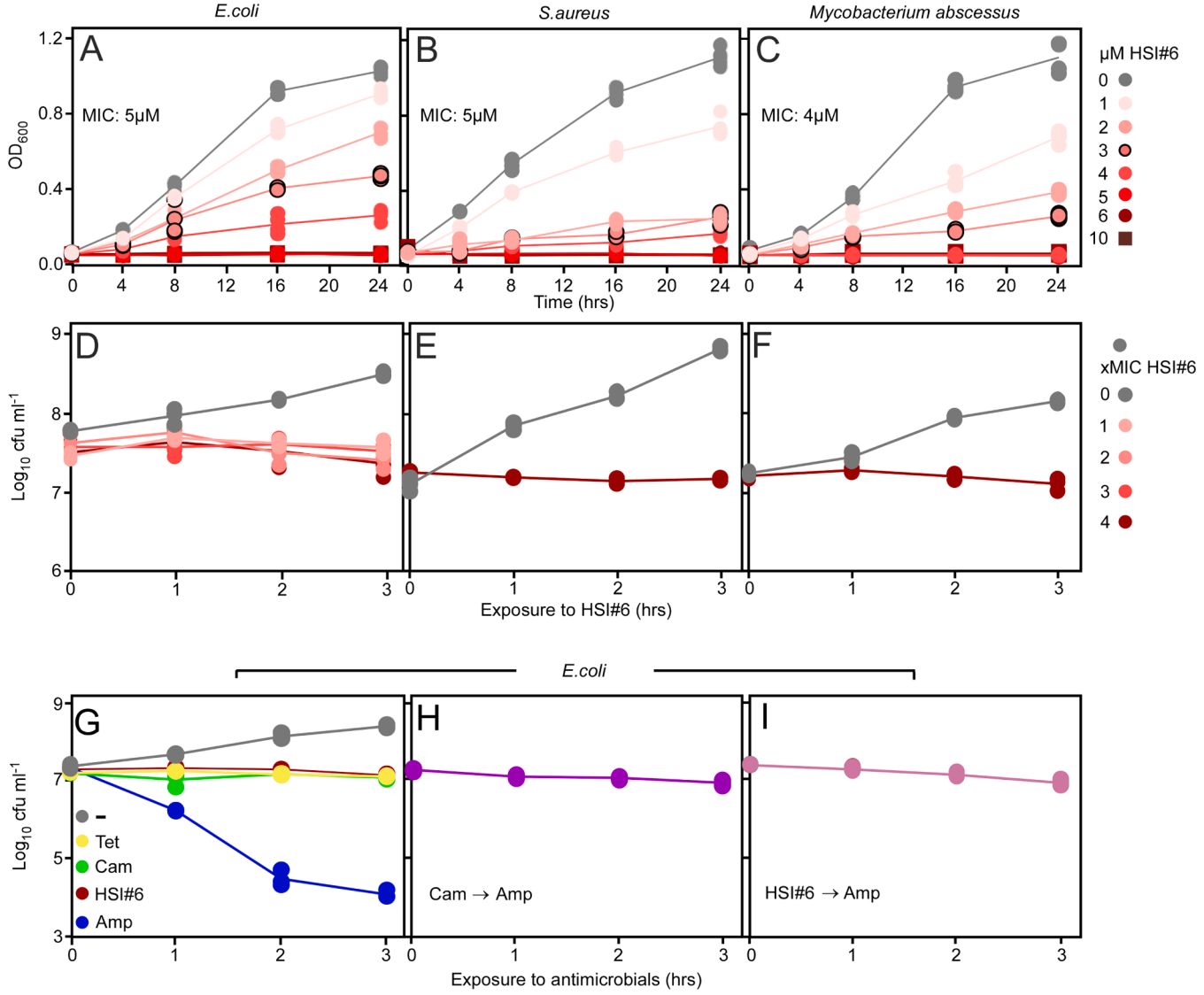

Fig. 1. HSI#6 is a rapidly acting bacteriostatic agent. A-C. Effect of HSI#6 (0–10 μM) on the growth rate of *E. coli* BW25113 (**A**), *Staphylococcus aureus* (**B**) and *Mycobacterium abscessus* (**C**). MICs are indicated. **D-F.** Time-kill assays using *E.coli* BW25113 (**D**) *Staphylococcus aureus* (**E**) and *Mycobacterium abscessus* (**F**). Freshly grown bacteria were diluted to OD_{600}=0.1, HSI#6 was added and the CFU / ml was determined at the indicated exposure times. **G-I.** Time-kill assays using *E.coli* BW25113 and the indicated antimicrobials (as in D-F). Chloramphenicol (Cam) / tetracycline (Tet) served as bacteriostatic examples; ampicillin (Amp) as a bactericidal one; no addition of antibiotics as control (**G**). Cells were treated with either Cam (**H**) or HSI#6 (**I**) for 20 min prior to Ampicillin addition. All antimicrobials were used at 4x MIC (6 μg/ml HSI#6; 5 μg/ml Amp; 15 μg/ml Cam; 10 μg/ml Tet). **A-I.** $n \geq 3$ independent biological repeats.

classification.

We have previously identified HSI#6, a small-molecule antibacterial (Hamed, Burchacka et al. 2021) that activates SecA-dependent protein secretion (Sedky, Hamed et al. 2026). In this study, we employ integrated omics approaches alongside functional assays to identify the mechanism of HSI#6 action. Specificity is evaluated by comparing the differences between the responses of a sensitive and a naturally resistant strain and by comparing the response to HSI#6 to the one against an inactive analogue. Our findings demonstrate that HSI#6 is a broad-spectrum bacteriostatic agent with a unique cellular response, distinct from any classical antibiotic mechanism, that shows some similarities to membrane acting agents such as monactin.

Results

HSI#6 is a rapidly-acting, broad-spectrum, bacteriostatic agent

HSI#6 is a potent antibacterial agent (Hamed, Burchacka et al. 2021). To determine its minimal inhibitory concentration (MIC), we studied the effect of various concentrations (0-20 μM) on the growth rate of *E.coli, Staphylococcus aureus* and *Mycobacterium abscessus*. Growth of all three strains, as well as that of an *E.coli* Δ*tolC* strain, was inhibited in a concentration dependent manner (Figs. 1A-C & Supplementary Fig. **1A**). Determined MICs ranged from 3-5 μM; the lowest one observed for the highly permeable *E.coli* Δ*tolC* strain. Addition of HSI#6 at MIC (5 μM) inhibited *E.coli* growth within 20 min of exposure, indicating a rapid drug uptake and onset of action (Supplementary Fig. **1B**).

To probe into the HSI#6 mode of action (MOA) time-kill assays were performed. Freshly grown cells were diluted to OD_{600}=0.1 (LB; 24-well plates), HSI#6 was added (1–4x MIC) and incubation continued (37 °C; shaking). At the indicated time following HSI#6 addition culture samples were serially diluted and 10 μl were plated on plain LB plates, incubated (37 °C; 12 hrs) and colony forming units (CFU / ml) were determined. We observe that for all strains the CFU / ml remained constant in the course of exposure time (Figs. 1D-F). This phenotype is similar to that of classic bacteriostatic antibiotics (chloramphenicol, tetracycline; 4x MIC; Fig. 1G) and unlike that of the bactericidal ampicillin, that decreased the CFU / ml by >3-log, at 3 hrs of exposure, at 4x MIC, consistent with previous reports (Lobritz, Belenky et al. 2015).

Bacteriostatic pretreatment is known to antagonize subsequent bactericidal activity (Ocampo, Lázár et al. 2014). In agreement to this, pretreatment of *E.coli* cells with either chloramphenicol or HSI#6 (4x MIC; 20 min) before ampicillin addition (4x MIC), protected *E. coli* from ampicillin-induced killing (Figs. 1H-I; compare to 1 G blue), consistent with previous results (Lobritz, Belenky et al. 2015). Similar results were observed for *S. aureus* (Supplementary Figs. **1C-D**).

Collectively, our results demonstrated that HSI#6 is a broad-spectrum, micromolar-potency bacteriostatic agent.

Genetic mutations increased E.coli tolerance to HSI#6

To evaluate the potential for resistance development the *E. coli* Δ*tolC* strain was gradually subjected to increasing HSI#6 concentrations. Initially cells were grown at 0.3 μM HSI#6 and over a six-month period the concentration gradually increased to 1 μM. After ~50 serial passages, 5 independent lineages reproducibly reached a stable, tolerant phenotype at 1 μM HSI#6. Growth of the sensitive ancestor at 1μM HSI#6 is compared to the growth of one tolerant lineage in Supplementary Figs **2A-B**. Despite multiple repeats, all lineages showed minor improvement at 1.5 μM and none at MIC (examples shown in Supplementary Figs **2C-D**) indicating limited tolerance rather than true resistance. The bacteriostatic nature of HSI#6 might impose low selective pressure, explaining the low evolutionary adaptation rate.

Whole-genome sequencing of the five lineages revealed a recurrent, missense mutation in *topA,* that was present in all lineages (A150E; Fig. 2A). *topA* encodes for topoisomerase I, a key enzyme for DNA topology regulation and transcription that has been correlated with stress adaptation and antibiotic resistance evolution (Bachar, Itzhaki et al. 2020; Dekker, Rybenkov et al. 2002; Kratz and Banerjee 2024; Tse-Dinh 2008; Usongo and Drolet 2014). In none of the 5 lineages *topA* mutation stood alone, it was combined with mutations in at least another gene. The latter included various types of mutations, distributed across coding regions / promoter elements and occurred in genes involved in transcriptional regulation (*rho, slyA, flhC*), fatty acid biosynthesis (*fabB, cfa*), fimbrium biogenesis (*fimE, fimA*), transport (*hsrA*), proteolysis (*clpA*), metabolism (*gltA, nudE, apbE*), toxin-antitoxin (*prlF*) and two component system (*atoC*) (Fig. 2A) (Alam, Bröms et al. 2021; Chen, Gong et al. 2023; Hafeezunnisa and Sen 2020; Jackowski, Zhang et al. 2002; Li, Jiang et al. 2020; Li, Plésiat et al. 2015; Yu, Yang et al. 2025). The encountered gene variety might be more consistent with a broad cellular adaptation response rather than a targeted resistance mechanism.

Nevertheless, to evaluate the contribution of *topA* into conferring HSI#6 tolerance, or as a target, an overexpression approach was employed (Palmer and Kishony 2014)·(Kitagawa, Ara et al. 2005). *topA* was cloned on a plasmid under the control of an IPTG-inducible promoter and transformed into *E. coli* BW25113 cells. IPTG was added at 50 μM, a concentration that minimally affected growth (Fig. 2B & Supplementary Fig. **2E**) and HSI#6 at MIC (5 μM). Despite *topA* overexpression, *E.coli* growth did not improve in the presence of HSI#6 (Fig. 2B) even at higher induction level, where IPTG concentrations increased up to 150 μM (Supplementary Fig. **2F**).

Taken our results together, it seems unlikely that *topA* is the direct target of HSI#6. We presume that the recurrent *topA* mutation likely represents a compensatory adaptation to stress, possibly via transcriptional modulation (Bachar, Itzhaki et al. 2020; Yang, Annamalai et al. 2015).

HSI#6 induces differential transcription in E. coli

To probe into the nature of the cellular response against HSI#6 we compared the transcriptomic profiles of *E. coli* BW25113 cells (LB; 37 °C; OD_{600}~0.2) that have been exposed for 30 min to addition of DMSO (0.2%), and either HSI#6 or the inactive analogue HSI#11 (3 μM; see Supplementary Note). While addition of HSI#11 did not alter transcription compared to DMSO (Supplementary Fig. **3A** & Supplementary Table **1**), HSI#6 addition did (Supplementary Fig. **3B** & Supplementary Table **1**), in agreement with a growth defect seen only in the presence of HSI#6, even in that narrow time-frame (Supplementary Fig. **3C**).

To characterize the response to HSI#6 in detail, the transcriptomic profiles of *E. coli* BW25113 cells exposed to either 3 μM HSI#6, or DMSO, for 5, 15, 30, 60 and 120 min, were compared and differential transcription was determined (Fig. 3A & Supplementary Table **1**). HSI#6 induced a rapid and extensive response. Within 5 min, the transcription of 407 genes was down-regulated and that of 302 genes up-regulated. The number of significant differentially expressed genes (sDEGs) increased with exposure time, peaking at 60 min, where ~half of the genome was affected, and declining by 120 min (for gene-identities see Supplementary Table **1**).

To further characterize the transcriptomic response we tracked the genes that appear at each time point, and followed their fate as a function of time. Several temporal changes were observed in the expression / composition of sDEGs (Figs. 3B-C & Supplementary Table **1**). Some were differentially expressed at early timepoints but not at later ones, while others only at later times. For example, from the 302 up-regulated genes seen at 5 min, 222 remained at 15 min while 259 new appeared additionally. It is intriguing, that >500 genes did not become up-regulated until 60 min of HSI#6 exposure, and another 98 not until 120 min (Fig. 3B & Supplementary Table **1**). Similar observations can be made with the down-regulated genes (Fig. 3C & Supplementary Table **1**).

This fine-tuned turnover likely reflects a highly specific

A

Gene	Mutation	Lineage(s)	Mutation type	Gene Function / involved in
topA	A150E	1 2 3 4 5	Missense	DNA topoisomerase I
fimE	G39R	1 2 5	Missense	Type 1 fimbriae regulatory protein
gltA	R164L	1	Missense	Citrate synthesis
Rho	R296S	4	Missense	Transcription terminator factor
fabB	C199F	5	Missense	Fatty acid synthesis
atoC	I129S	3	Missense	Two-component AtoS/AtoC
ApbE	Q170*	2	Stop	Flavin transferase
slyA	Early ORF	5	Frameshift	Transcription regulator
clpA	Early ORF	5	Frameshift	ATP-dependent protease
prlF	Early ORF	3	Frameshift	Component of type II toxin - antitoxin system
nudE	Early ORF	1	In-frame deletion	ADP hydrolase
hsrA	Promoter	1	Upstream transcript regulation	Putative efflux pump
cfa	Promoter	2		Cyclopropane-fatty-acyle phospholipd synthase
flhC	Promoter	4		Flaggelar transcriptional regulator
fimA	Promoter	3		Type-1 fimbrial protein

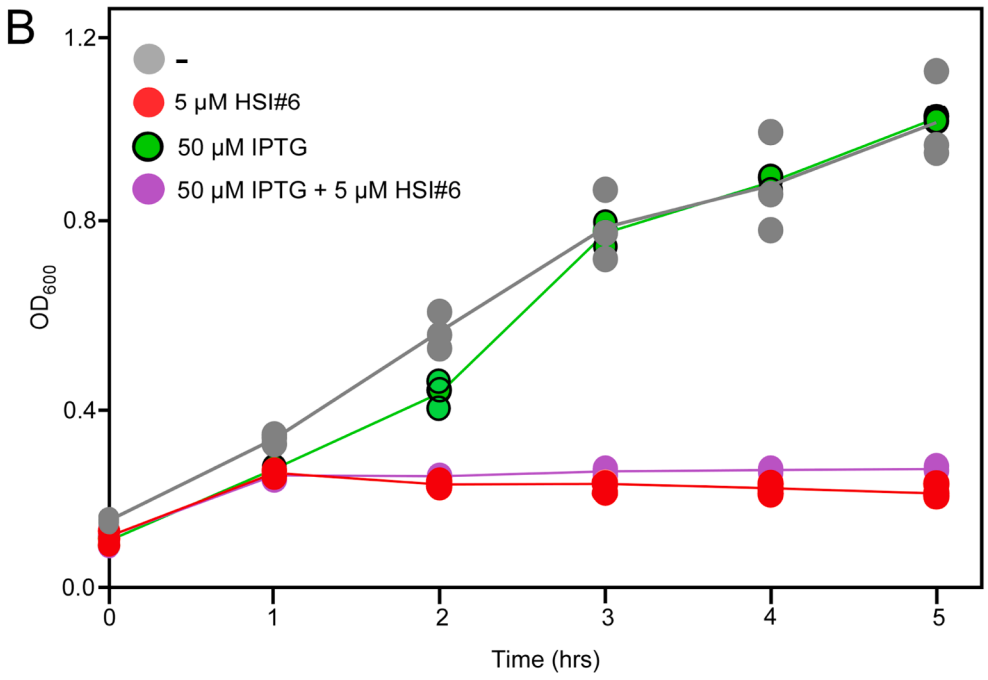

Fig. 2. HSI#6 developed tolerance in *E. coli* Δ*tolC*. A. Mutations identified in *E.coli* BW25113 Δ*tolC* isolates of five independent lineages, that exhibited higher tolerance in HSI#6 than the mother strain, are listed. The mutated gene(s) per lineage, location, type of mutation, frequency and gene function are indicated. **B.** Effect of overexpressing *topA* from a plasmid (50μM IPTG\0 on the growth of *E. coli* BW25113, in the absence (green) / presence of 5 μM HSI#6 (purple). Control experiments with neither IPTG nor HSI#6 (grey), or with only 5 μM HSI#6 (red) are shown. $n \geq 3$.

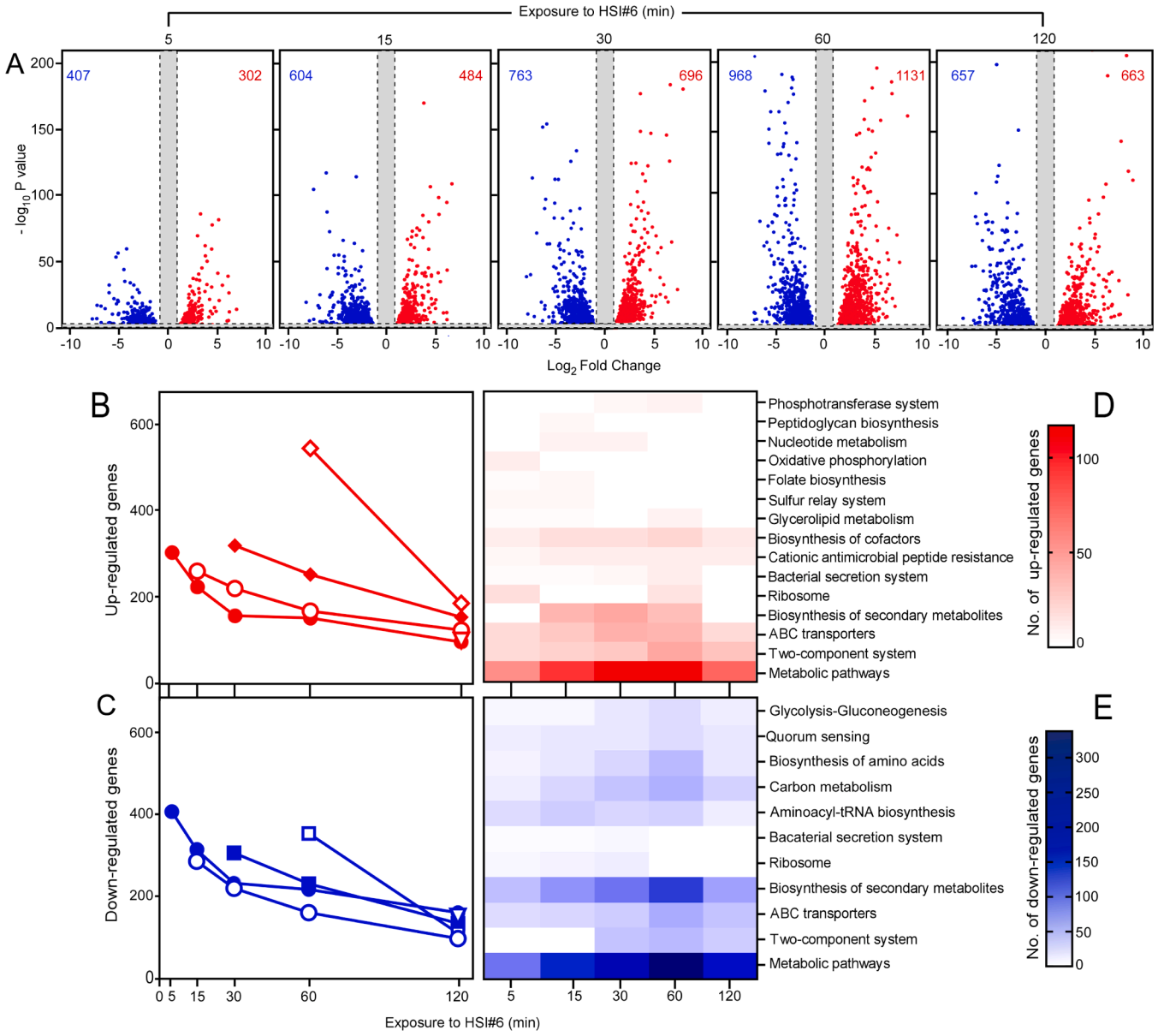

Fig. 3. HSI#6 alters the transcriptomic profile of *E. coli*. A. The differential transcriptomic profile between *E. coli* BW25113 cells exposed to HSI#6 and cells exposed to an inactive analogue under identical conditions, in the course of exposure time, is shown by Volcano plots. The number of up- (red) / down- (blue) regulated genes at each time point is indicated. $n = 3$. **B-C.** Time of first appearance and number of DEGs in response to HSI#6 and their fate in the course of exposure time; red / blue = up- / down- regulated respectively. **D-E.** Pathways and number of genes per pathway that become differentially regulated, at each time point following addition of 3 μM HSI#6, according to KEGG analysis; up- (**D**) / down- (**E**) regulated genes.

transcriptional reprogramming / regulation in response to a continuous stress. In agreement to this hypothesis, we observe activation of (Supplementary Table **1**): **i.** the σ^{32}-heat-shock system (e.g. *dnaK, dnaJ, clpB, htpG, ibpA/B*) indicative of acute proteotoxic stress (Matuszewska, Kuczyńska-Wiśnik et al. 2005; Thomas and Baneyx 1998); **ii.** all five envelope-stress pathways (σ^E, Cpx, Rcs, Bae, Psp) with marked differential expression of signature genes (e.g. *cpxP, spy, tolABQR, fkpA, bamE, osmB, osmY, wzc; baeS, tolC, mdtAB; pspA/E*) indicative of cell envelope damage in line with previously reported findings (Bury-Moné, Nomane et al. 2009); **iii.** outer-membrane remodeling (e.g. *lamB, ompC, ompF, phoE*); **iv.** oxidative-stress regulators (e.g. *soxR, soxS, oxyS*); **v.** SOS DNA-damage associated genes (e.g. *recA, lexA umuCD, sulA, uvrBC*) (Mo, Culyba et al. 2018; Nunoshiba, Hidalgo et al. 1992). This stress signature coincided with global downregulation of translation, *via* suppression of ribosomal protein genes (e.g. *rpsU, rplU, rpmA*), and repression of central carbon metabolism (e.g. *gapA, pykF, aceA/B/K*), indicating a broad metabolic slowdown (see also below).

To examine whether the cellular response against HSI#6 involves sDEGs enrichment of specific biological pathways, the Kyoto encyclopedia of genes and genomes (KEGG) analysis was used (FDR:0.05; 20 most significant pathways; sort by genes). Results are presented using a color-gradient-code to indicate the number of sDEGs per pathway, relative to time of HSI#6 exposure (red / blue = up- / down- regulated respectively). For example, for ABC transporters, 18 genes became up-regulated at 5 min, 29 at 15 min, 39 at 30 min and then at 60 min they decreased to 19. Metabolic pathways, two-component system, ABC transporters, ribosomes, bacterial secretion systems and biosynthesis of secondary metabolites are affected by both up- and down- gene regulation (Figs. 3D-E). Pathways affected exclusively by gene-upregulation include cationic antimicrobial resistance, biosynthesis of cofactors / peptidoglycan / folate, nucleotide / glycerolipid metabolism, oxidative phosphorylation, phosphotransferase and sulfur relay systems (Fig. 3D).

Those affected only by gene-downregulation include tRNA biosynthesis, carbon metabolism, biosynthesis of amino acids, quorum sensing and glycolysis (Fig. 3E).

HSI#6 alters the E.coli proteomic profile

Next, we performed quantitative proteomic analysis of *E. coli* BW25113 cells that have been exposed to HSI#6, or HSI#11 (3 μM), or DMSO. As anticipated from the antibacterial activity and the transcriptomic study (Supplementary Fig. **3**), HSI#11 did not induce differential expression of proteins (DEPs), while HSI#6 did (Supplementary Table **2**).

To mirror our proteomic study to the transcriptomic one, we determined the proteomic profile of *E. coli* BW25113 in the course of time (15, 30, 60, and 120 min) following 3 μM HSI#6 addition; the proteomic response to 3 μM HSI#11 addition was used as control. The determined differential proteomic profiles (Fig. 4A; for protein identities see Supplementary Table **3**) reveal changes in the protein expression that were limited at early time points and more extensive at later time points (Aita, Ristori et al. 2025; Torres-Sangiao, Giddey et al. 2022). Temporal changes were observed in the differential abundance / composition of proteins as well (Figs. 3B-C & Supplementary Table **3**). However, these are less pronounced compared to the transcriptomic changes (compare Figs. 4B-C to 3B-C). The proteomic response seems evidently delayed relative to the transcriptomic one; the former continues to increase at 120 min while the latter is already on the decline by

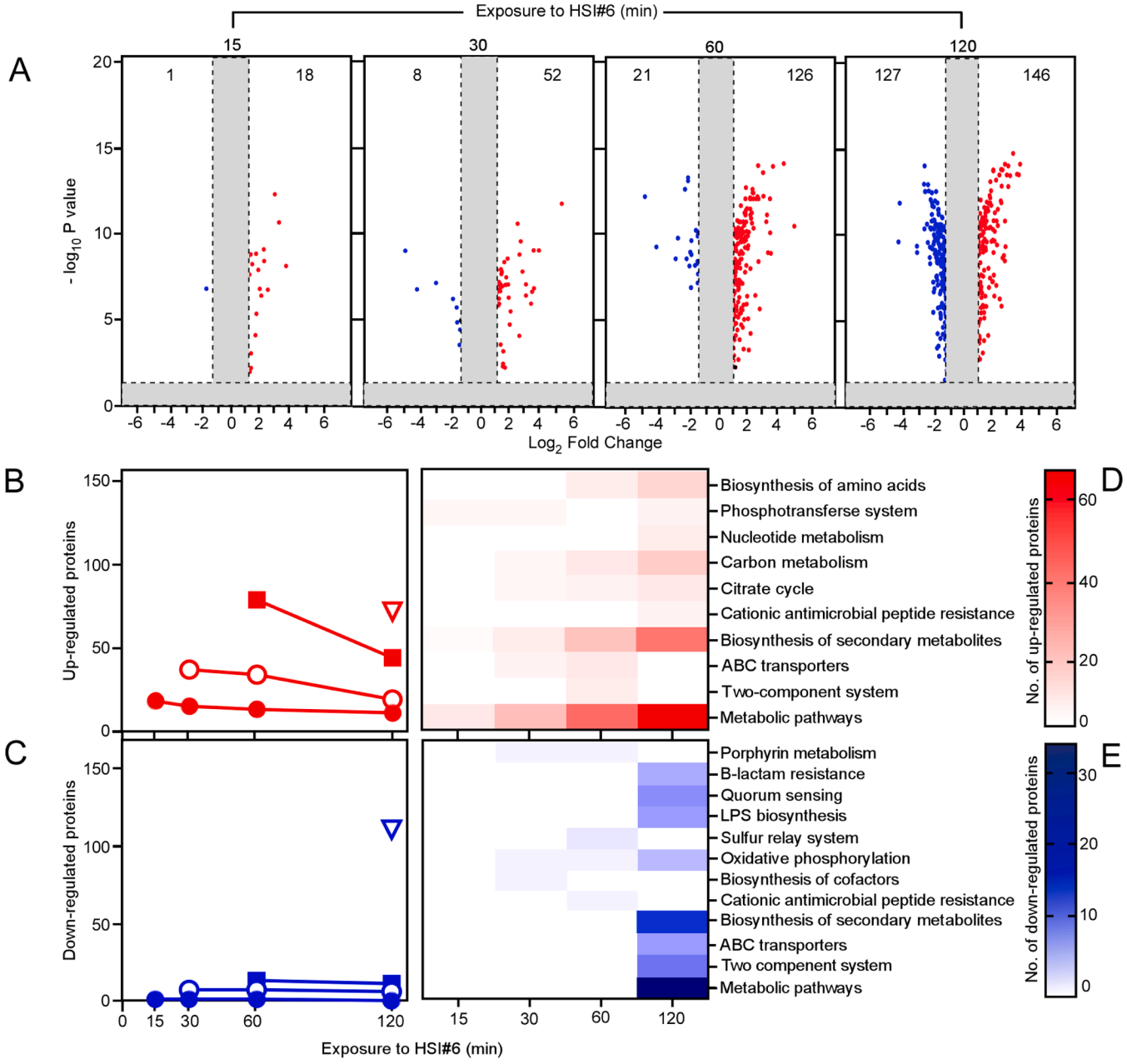

Fig. 4. HSI#6 alters the proteomic profile of *E.coli*. A. The differential proteomic profile between *E. coli* BW25113 cells exposed to HSI#6 and cells exposed to an inactive analogue under identical conditions, in the course of exposure time, is shown by Volcano plots. The number of up- (red) or down- (blue) regulated proteins at each time point is indicated. $n = 3$. **B-C.** Time of first appearance and number of differentially expressed proteins in response to HSI#6 and their fate in the course of exposure time; red / blue = up- / down- regulated respectively. **D-E.** Pathways and number of proteins per pathway that become differentially expressed, in the course of time, following addition of 3 μM HSI#6, according to KEGG analysis; up- (**D**) / down- (**E**) regulated proteins.

then (compare Figs. 4A-C to 3A-C).

Among DEPs (Supplementary Table **3**) there is a strong enrichment of stress-response / proteostasis factors (e.g. IbpA/B, ClpA/B, RpoH, RaiA, RMF), consistent with activation of protein-quality-control systems (Lang, Krin et al. 2021; Matuszewska, Kuczyńska-Wiśnik et al. 2005; Thomas and Baneyx 1998). Upregulation of CpxP, nutrient-uptake components (e.g. MalF/G/K, GlpF/K, UgpB, NupG) and envelope-associated proteins (e.g. YhcN, BhsA) indicated activation of Cpx / σ^E -type envelope stress responses (Boos and Shuman 1998; Pettigrew, Ma et al. 1988; Schweizer and Boos 1984; Wang, Xiao et al. 2021; Wood 2009). The parallel increase in oxidative-stress defense proteins (e.g. SoxS, SodC, GrxB, MsrA, KatE) suggested enhanced redox protection (Jung and Kim 2003; Moskovitz, Rahman et al. 1995; Potamitou, Neubauer et al. 2002). In contrast, hallmark energy-linked functions were broadly depleted, including cold-shock proteins (CspA/B/G), cytochrome oxidase subunits (CyoA/B/E), and several TCA-cycle and respiratory-chain enzymes (Borisov Vitaliy and Verkhovsky Michael 2015; Etchegaray and Inouye 1999).

KEGG pathway analysis (as in Figs. 3D-E) shows that for at least some of the changes, proteomics and transcriptomics seem to agree. For example, the differential protein enrichment in metabolic pathways, two component system, ABC transporters, biosynthesis of secondary metabolites and cationic antimicrobial resistance seem to mirror a transcript-level activation (compare Fig. 4D to 3D). Others appear uniquely in one or the other response. For example, folate biosynthesis, sulfur relay system and glycerolipid metabolism, pathways with enriched DEGs in transcriptomics do not show up in proteomics or, the citrate cycle, carbon metabolism and phosphotransferase system are pathways that seem enriched in proteomics but not in transcriptomics (compare Fig. 4D to 3D). Similar observations can be made with the down-regulated genes (compare Fig. 4E to 3E).

The E.coli transcriptomic response against HSI#6 is distinct and aligns best with known ionophore-like antibiotics

To classify the molecular mechanism of HSI#6 action, the transcriptomic profile of *E.coli* BW25113 was compared with those induced by 37 conventional antibiotics, known to target various cellular processes (O'Rourke, Beyhan et al. 2020). Pearson correlation coefficients were calculated using values of overlapping DEGs (Supplementary Table **4**). Correlation values ranged from 0–1 and are visualized as a global correlation heatmap using a gradient color code that ranges from white to red respectively (Fig. 5A). HSI#6 exhibited its strongest transcriptional similarity to the membrane-active ionophore monactin, with a moderate correlation coefficient (r = 0.48, at 30 min). Weaker correlations were observed with fatty acid synthesis inhibitors ($r_{cerulenin}$= 0.34; $r_{isoniazid}$= 0.26) and DNA damage inducers ($r_{metronidazole}$= 0.29). To ensure that this classification was not confounded by temporal variation in stress intensity, correlations were calculated also for all HSI#6 exposure times (5–120 min). Monactin consistently remained the highest-correlating compound (Supplementary Table **4**).

Since a 447-gene-biomarker set has been previously shown to accurately classify the molecular mechanism of antibiotic action (O'Rourke, Beyhan et al. 2020), we repeated our analysis using it. Correlations derived using the biomarker set mirrored the whole-transcriptome comparisons across time points, and identified monactin as the highest one (r = 0.51; Fig. 5A, as indicated & Supplementary Table **4**). An increased correlation with actinomycin D was observed at 60 min, consistent with prior reports positioning actinomycin D near monactin within comparative transcriptomic space (O'Rourke, Beyhan et al. 2020). However, this correlation did not surpass that of monactin and did not persist across time points. Taking these findings further, we correlated sDEGs in response to HSI#6 and monactin and found that their correlation increased from moderate to high (r = 0.88; Supplementary Fig. **4A**).

KEGG pathway analysis revealed a distinct functional signature for HSI#6, relative to other antibacterials. Some genes were solely up / down -regulated in response to HSI#6 and not to other antibacterials. Unique to HS#6, up-regulated genes fall in metabolic pathways, two component system, bacterial secretion system and flagellar assembly, whereas unique down-regulated ones in metabolic pathways, biosynthesis of secondary metabolites, and quorum sensing (Supplementary Fig. **4B**). Nevertheless, some pathways enriched in sDEGs are shared between HSI#6 and monactin (Supplementary Fig. **4C**), suggesting some functional similarities between them.

The E.coli proteomic response against HSI#6 is distinct and aligns best with antibiotics that cause cell envelope perturbation

To see how the molecular mechanism of HSI#6 action would be classified based on the proteomic response, we first examined how the global RNA response relates to its corresponding protein output using Pearson correlation coefficients (as in Fig. 5A). Comparison of $\log_2$ fold-change values revealed only a weak correlation between the transcriptomic and proteomic responses (r = 0.25; Fig. 5B), reflecting the known decoupling of RNA and protein abundances during antimicrobial stress due to extensive post-transcriptional and translational regulation (Jensen, Zhu et al. 2017; Yu, O'Rourke et al. 2020).

Next, we used principal component analysis (PCA) to compare the proteomic response of an HSI#6-treated sensitive strain against reference antibiotics by the $\log_2$ fold change of 14 protein-biomarkers, known-predictive-indicators-of-the-antibiotic-action-mechanism (Yu, O'Rourke et al. 2020). The expression of these biomarkers captures stress signatures associated with major antibiotic classes, including cell envelope-targeting agents (CE), protein synthesis inhibitors (PS), and fatty acid synthesis inhibitors (FAS).

Based on this analysis the antibacterials used were clustered in three distinct groups (Fig. 5C): **a.** The PS cluster (green) represented inhibitors of translation / transcription and included tetracycline (TCH), erythromycin (ETM), retapamulin (RTP) and related agents; **b.** The FAS cluster (yellow), consistent with fatty acid biosynthesis inhibition, included triclosan (TCS), isoniazid (INA) and cerulenin (CEL); **c.** The CE cluster (blue) represented membrane-active / cell wall-targeting antibiotics including polymyxin B (PMB), penicillin (PEN), monactin (MNA), ceftriaxone (CTA), cefotaxime (CFA) and flavomycin (FVM). The response of *E.coli* BW25113 to HSI#6 was positioned nearest to the CE cluster, confirming higher correlation/ resemblance to membrane-active agents rather than inhibitors of protein or fatty acid synthesis, in agreement to conclusions derived from the transcriptomics comparison.

HSI#6 fails to elicit a detectable molecular response in resistant EPEC

Finally, to further validate our study we used as control the naturally resistant to HSI#6 enteropathogenic *E.coli* (EPEC) strain (Hamed, Burchacka et al. 2021) (compare Supplementary Fig. **5A** to Fig. 1A). This reduced susceptibility of EPEC is consistent with its documented antibiotic resistance potential (Gambushe, Idowu et al. 2026).

We recorded both the transcriptional as well as the proteomic responses of EPEC to HSI#6, or HSI#11 as control (10 μM; 30 min; as in Figs. 3–4). In contrast to the sensitive *E. coli* BW25113 strain, EPEC displayed only minimal transcriptomic alterations upon HSI#6 exposure (33_{EPEC} vs $1495_{E.coli}$; compare Supplementary Fig. **5B** to Fig. 3A, 30min; Supplementary Table **5**). A similarly limited response was observed at the protein level, with only two significantly altered proteins following HSI#6 treatment (10 μM; 30 min; Supplementary Fig. **5C** & Supplementary Table **5**).

To directly compare the resistant (EPEC) and sensitive (*E.coli* BW25113) backgrounds, we correlated their responses at the RNA and protein level, calculating Pearson correlation coefficients, as in Fig. 5A. The transcriptomic signatures of EPEC and BW25113 are weakly related (r = 0.18; Supplementary Fig. **5D**). Likewise, poor similarity was observed between the proteomic responses of EPEC and *E.coli* BW25113

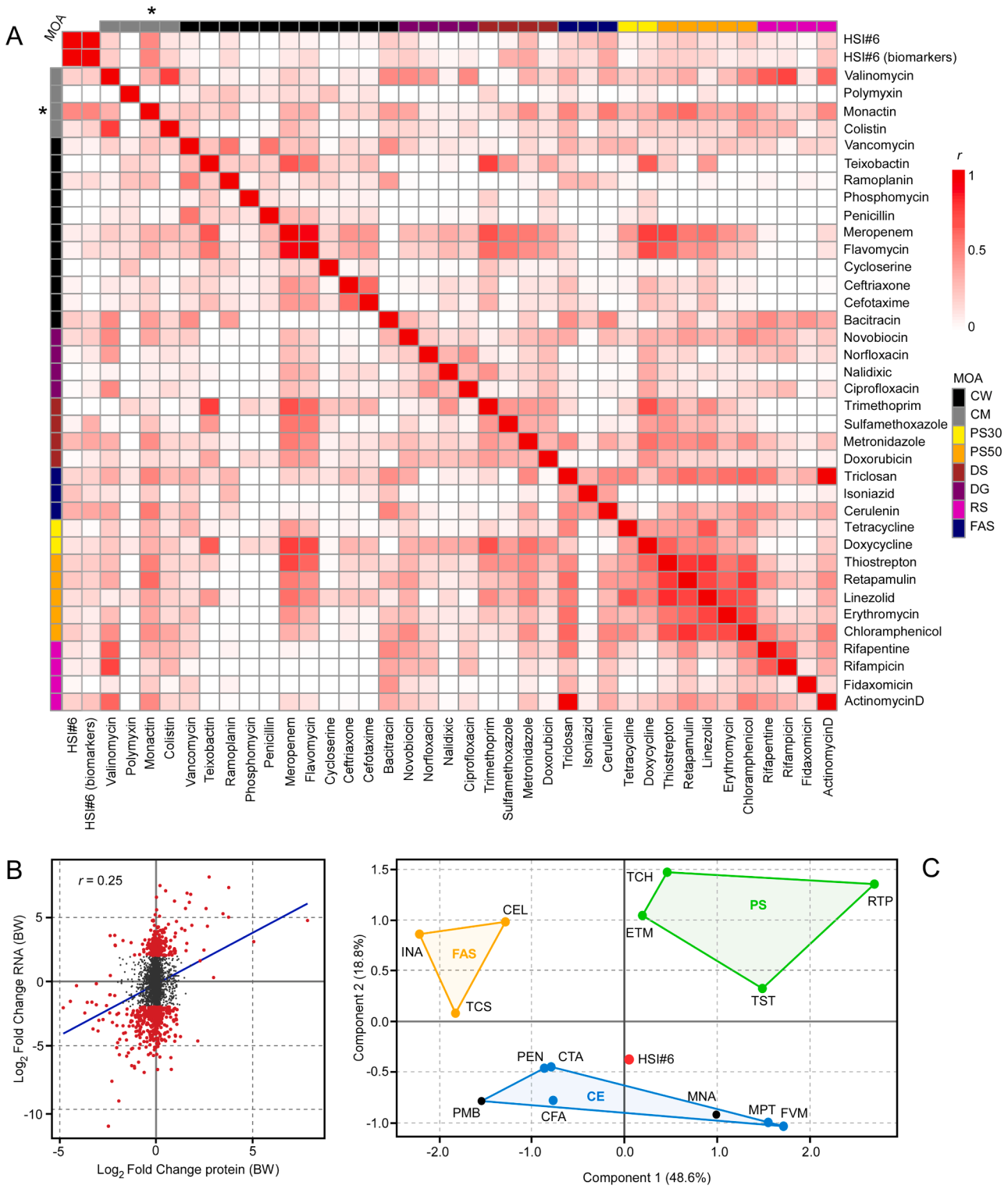

Fig. 5. Comparison of the *E.coli* HSI#6-response to known antimicrobial-responses. A. The transcriptome of the *E.coli* BW25113, at 30 min following addition of HSI#6 (3 μM), is compared pairwise to that of the indicated antibiotics that belong to different classes (indicated by color code) and affect: cell wall (CW), cell membrane (CM), protein synthesis 30 s ribosomal subunit (PS30), protein synthesis 50 s ribosomal subunit (PS50), DNA synthesis (DS), DNA gyrase (DG), RNA synthesis (RS) and fatty acid synthesis (FAS). The correlation strength between two antimicrobials is shown by a gradient color code, ranging from 0 (white, no correlation, negative) to 1 (red, highest correlation). The comparison was based on DEGs (HSI#6), or 447 genes (HSI#6 biomarkers). An asterisk indicates the highest correlation of HSI#6 to monactin. **B.** Pearson correlation (*r*) between the transcriptomic and proteomic response of *E.coli* BW25113, at 30 min following addition of 3 μM HSI#6. **C.** Principal component analysis (PCA) was used to cluster the response of *E.coli* to the indicated antimicrobials based on the expression pattern of 14 protein-biomarkers. Three antibiotic classes were formed affecting fatty acid synthesis (FAS; yellow; cerulenin, triclosan and isoniazid), protein synthesis (PS; green; tetracycline, erythromycin, thiostrepton and retapamulin) and cell envelope (CE; blue; cell wall: ceftriaxone, penicillin, cefotaxime and flavomycin; cell membrane: monactin and polymyxin). Using the same analysis HSI#6 (red) is positioned closer to the CE cluster.

($r = 0.13$; Supplementary Fig. **5E**).

Overall, the minimal transcriptomic and proteomic changes in EPEC provided a useful negative control, demonstrating that HSI#6 does not induce a measurable cellular response in the resistant background and reinforcing the specificity of the extensive response observed in the susceptible strain.

Discussion

The rise of bacterial antibiotic resistance demands the development of new drugs with novel mechanisms of action to minimize cross-resistance (Butler, Vollmer et al. 2024; Piddock, Malpani et al. 2024). In this context, our study provides a comprehensive mechanistic profile of HSI#6, a small-molecule antibacterial that was also previously shown to activate the Sec protein secretion system (Hamed, Burchacka et al. 2021; Sedky, Hamed et al. 2026). By combining integrated omics with functional assays, we show that HSI#6 exerts its antibacterial activity through a mechanism associated with envelope perturbation, broad stress reprogramming, and has low propensity for resistance development.

HSI#6 exhibited broad-spectrum bacteriostatic activity against Gram-negative / positive bacteria including *Mycobacterium abscessus*, with rapid growth inhibition and no lytic effect (Fig. 1). Time-kill assays, the antagonism of bactericidal activity upon pretreatment with HSI#6, and the variable growth-inhibitory effect at subinhibitory concentrations confirmed a classic bacteriostatic behavior (Lobritz, Belenky et al. 2015; Ocampo, Lázár et al. 2014; Vaisbourd, Glass et al. 2025). These findings indicate that HSI#6 primarily targets a conserved pathway essential for bacterial growth.

Several attempts to evolve resistance under stepwise increase in HSI#6 concentration yielded only modest gain in tolerance, whereas whole-genome sequencing repeatedly identified mutations in *topA* and in transcriptional regulators such as *fimE, rho, slyA*, and *prlF*, together with changes in genes linked to fatty-acid metabolism and efflux control (Fig. 2A). This pattern is more consistent with compensatory adaptation to drug-induced stress than with simple target-site escape through a single high-impact mutation. One possible explanation is that HSI#6 perturbs an essential and highly constrained cellular pathway, making direct resistance by target modification less accessible. The recurrent emergence of *topA* mutations is notable, as bacterial topoisomerase I plays a central role in maintaining DNA topology during transcription and stress adaptation and has been proposed as a promising antibacterial target (Aswal, Singh et al. 2025; Tse-Dinh 2008).

Integrated omics analyses uncovered the complexity of the HSI#6 molecular mechanism of action. Despite discrepancies between transcriptomic and proteomic outputs, that can arise either from the higher sensitivity of transcriptomics, or the delay in protein-level responses, or a regulation occurring primarily at the translational level (Jensen, Zhu et al. 2017, Yu et al., 2020, O'Rourke et al. 2020), the proteomics broadly recapitulated the major transcriptomic trends. In summary, HSI#6 provoked a rapid response that among others affected expression of : **i.** members of the Cpx / σ^E stress regulons associated with cell envelope homeostasis (Boos and Shuman 1998; Bury-Moné, Nomane et al. 2009; Pettigrew, Ma et al. 1988; Schweizer and Boos 1984; Wang, Xiao et al. 2021; Wood 2009) ; **ii.** members of heat-shock chaperone network, typically involved in protein-misfolding / aggregation stress (Matuszewska, Kuczyńska-Wiśnik et al. 2005; Thomas and Baneyx 1998); **iii.** oxidative stress regulators and SOS DNA-damage response (Mo, Culyba et al. 2018; Nunoshiba, Hidalgo et al. 1992); **iv.** genes involved in oxidative / redox -triggered genomic stress (Jung and Kim 2003, Potamitou, Neubauer et al. 2002). These are combined with widespread repression of translation and central metabolism (including glycolysis / TCA cycle / nucleotide and fatty-acid biosynthesis / oxidative phosphorylation (Supplementary Table **1**). KEGG analysis (Figs. 3D-E & 4D-E) confirmed that the majority of gene expression changes are consistent with a shift into a lower-energy protective state (Borisov Vitaliy and Verkhovsky Michael 2015; Etchegaray and Inouye 1999), reflecting the metabolic reprogramming that accompanies a bacteriostatic antibiotic stress (Ahmad, Aduru et al. 2025; Zhu and Dai 2020).

Omics analyses not only detailed the response against HSI#6, they allowed for its direct comparison to the cellular responses against 37 known antimicrobials, each one with different molecular mechanism of antimicrobial action. Our analysis identifies HSI#6 as a distinct antibacterial that aligns best with antibiotics that induce a cell-envelope stress response (Fig. 5). Given its physicochemical properties, e.g. lack of a positive charge (Supplementary Note), its bacteriostatic mode of action with no lytic effect (Fig. 1) and low SI [calculated as in (Xu, Wang et al. 2026; Xu, Yan et al. 2026)], it seems unlikely that HSI#6 acts through membrane binding and disruption. The correlation of HSI#6 response to that of membrane-active antibiotics may simply reflect generalized envelope stress response, including altered secretion. Although the link between HSI#6-antibacterial activity and allosteric activation of SecA-dependent secretion (Sedky, Hamed et al. 2026) needs further investigation, our study highlights the potential of targeting underexplored processes, such as protein secretion and envelope homeostasis. The distinct HSI#6-omics signature, multifaceted response, and low resistance-development support its value as a mechanistic antibacterial lead and demonstrate the utility of integrated omics for mechanism-guided antibiotic discovery. Nevertheless, future studies are required to assess the HSI#6 impact on membrane potential, envelope morphology, hemolysis, along with a detailed preclinical evaluation of its cytotoxicity, pharmacokinetics and in vivo efficacy, beyond what has been reported already (Supplementary Note),

Materials and methods

Strains and growth conditions

The following bacterial strains were used: *S. aureus* (ATC6538P), *E. coli* K12 (BW25113; BW25113Δ*tolC*), Enteropathogenic *E. coli* O127: H6 (E2348/69 / EPEC) and *Mycobacterium abscessus* (ATCC19977). For *S.aureus* and *E.coli* LB medium was used; for *Mycobacterium abscessus* tryptic soya broth (TSB).

MIC determination

As described (Wiegand, Hilpert et al. 2008). Briefly, bacterial cultures, standardized to 5×10^5 colony forming units (CFU) / mL, were exposed to a range of antimicrobial concentrations, for 16–24 h, at 37 °C, before OD_{600} was recorded. The MIC value was identified as the lowest antimicrobial concentration required to inhibit bacterial growth.

Time kill assays

As described (Barry 1999). Overnight cultures were diluted 1:200 into 50 mL of fresh media, in a 250-mL flask and grown at 37 °C, ~180 rpm, to early log phase. Cells were transferred into a 24-well dish, their OD_{600} was adjusted to ~0.1 using LB, the indicated antimicrobial was added and growth continued at 37 °C under shaking. At the indicated time following this addition, or / and a second antibiotic/ vehicle control addition (as indicated), 300 μL culture was sampled, 10-fold serially diluted and 10 μL drops were plated on drug-free LB agar. Plates were incubated (18–24 hrs; 37 °C) and colonies (CFU / mL) were measured.

Isolation/identification of mutations that confer HSI#6 tolerance to E.coli cells

As described (Usui, Yoshii et al. 2023). An adaptive laboratory evolution regimen was applied to *E. coli* BW25113ΔtolC strain to select for cells that showed increased tolerance to HSI#6. Cells were initially grown at 0.3 μM HSI#6 and over a six-month period HSI#6 gradually

increased to 1 μM. After 50 serial passages, 5 independent evolutionary lineages reproducibly reached a stable, tolerant phenotype at 1 μM HSI#6. Cultures from each lineage were streaked on LB agar to obtain single colonies. One tolerant isolate from each of the five independent lineages was selected for characterization. From each isolate, genomic DNA was extracted using a DNA purification kit according to manufacturer's instructions (Thermo Fisher Scientific), that yielded high-molecular-weight DNA suitable for next-generation sequencing library preparation. Whole-genome sequencing was performed using an Illumina MiSeq platform with a paired-end 150 bp sequencing configuration, targeting an average sequencing depth of approximately 100×. Single-nucleotide variants (SNVs), including single-nucleotide polymorphisms (SNPs), small insertions and deletions (indels) and copy-number variations (CNVs) were identified using NGSEP (version 3.3.1) (Duitama, Quintero et al. 2014). For variant calling the following parameters were used: -runRep, -RunRD, -RunRP, -maxBaseQS 30, -minQuality 40, and -maxAlnsPerStartPos 2. The resulting variant call format (VCF) files were annotated using the corresponding GFF3 annotation file obtained from NCBI and associated with the reference genome FASTA file. SNVs that differed from both the reference genome and the parental strain were extracted through filtering and compiled for further analysis. For SNPs located within open reading frames (ORFs), the reference and alternative nucleotides, genomic position, affected gene, and resulting amino acid substitution were recorded. SNPs located outside ORFs were classified based on genomic context, promoter regions, terminator regions, or intergenic regions. Small indels were annotated according to genomic location and predicted effect, including in-frame or frameshift mutations within ORFs and indels occurring in promoter regions. CNVs were identified by comparing sequencing coverage across the genome and regions displaying altered copy number were defined by their genomic start and end positions and the relative increase in average coverage compared to the genome-wide baseline (1×). The tolC deletion was detected in all sequenced isolates.

RNA extraction

Bacteria were treated with either 0.2% DMSO or with, HSI#6 or HSI#11 (for *E. coli* BW25113 compounds were at 3 μM; for EPEC at 10 μM), and RNA was extracted using the NucleoSpin RNA kit (MACHEREY-NAGEL, cat. 740,955) following the manufacturer's instructions. Lysis was achieved by addition of buffer RA1 supplemented with β-mercaptoethanol and the lysate was cleared using a NucleoSpin filter. 70% ethanol was added, followed by on-column rDNase digestion, sequential washes and elution in RNase-free water. RNA quality was assessed using the Bioanalyzer 2100 (Agilent Technologies) with the Agilent RNA 6000 Nano Kit (Cat. No. 5067–1511) according to manufacturer's protocol. Libraries were prepared using the NEBNext Ultra II Directional RNA Library Prep Kit for Illumina (96 reactions; Cat. No. E7760L; Bioké). Ribosomal RNA was depleted using the NEBNext rRNA Depletion Kit v2 (Bacteria) with beads (24 reactions; Cat. No. E7860L; Bioké) to remove 16S/23S rRNA prior to cDNA synthesis. Standard steps included reverse transcription, second-strand synthesis, end repair, adapter ligation and PCR enrichment. Libraries were pooled and sequenced on an Illumina NovaSeq 6000 in single-read mode using one lane of a non-shared flow cell.

Transcriptomic analysis

For quality control of raw reads FastQC v.0.11.9 was used (S. 2010). Adapters were filtered using Trimmomatic v.0.39 (Bolger, Lohse et al. 2014). Splice-aware alignment was carried out using Hisat2 v.2.2.1 (Kim, Paggi et al. 2019), against the reference genomes of *E.coli* BW25113 (accession: NZ_CP009273.1) or *E. coli* EPEC E2348/69 (NCBI accession: NC_011601.1), with the transcriptome version employing default mapping parameters. For quantification of reads per gene the FeatureCounts v.1.5.1 from the Subread package was used (Liao, Smyth et al. 2013). For count-based differential expression analysis the R-based Bioconductor package DESeq2 was used. Reported p-values underwent adjustment for multiple testing using the Benjamini-Hochberg procedure to control for false discovery rate (FDR). Genes were considered differentially expressed if the adjusted P-value ≤ 0.05 and $|\log_2 \text{fold change}| \geq 1$ (i.e. at least a two-fold difference between conditions). For visualization volcano plots were used, where $\log_2$ fold change was plotted against - $\log_{10}$ adjusted P-value to highlight significantly up- / down- regulated genes.

Proteomic analysis

Bacteria were treated with either 0.2% DMSO or with, HSI#6 or HSI#11 (for *E. coli* BW25113 3 μM compound was used; for EPEC 10 μM) and lysed by using the radioimmunoprecipitation assay (RIPA buffer #R0278, Sigma-Aldrich) according to manufacturer's instructions. Protein concentration was determined using the Pierce bicinchoninic acid protein assay kit (#23,227, Thermo Fisher Scientific). Samples were analysed using liquid-chromatography-mass-spectrometry (LC-MS; loading 50 μg of total protein / sample) and the S-Trap micro sample prep kit (K02-micro-160, ProtiFi, Fairport, NY, USA) according to manufacturer's instructions. Briefly, samples were solubilized in 5% (w/v) sodium dodecyl sulfate (included in the prep kit), reduced by 5 mM tris-(2-carboxyethyl)-phosphine (#75,259, Sigma-Aldrich), alkylated by 20 mM iodoacetamide (#I1149, Sigma-Aldrich), and denatured further with 2.5% (v/v) phosphoric acid (452,289, Sigma-Aldrich). Samples were loaded on S-trap columns for purification, and proteins were digested with trypsin (#V511A, Promega, Madison, WI, USA; 1 μg / 50 μg protein). Peptides were eluted using sequentially three different elution buffers [50 mM triethylammonium bicarbonate (90,114, Thermo Fischer Scientific); 0.2% (v/v) formic acid (84,865.260, VWR, Leuven, Belgium); and 50% (v/v) acetonitrile (#83,640.320, VWR)] and dried using speed vacuum centrifugation. Lyophilized peptides were reconstituted in solvent A [H_2O, 0.1% (v/v) formic acid] and ~200 ng / sample were loaded onto an Evotip Pure tip (Evosep, Odense, Denmark). Peptide mixtures were analyzed using an Evosep One LC (Evosep) coupled to a ZenoTOF 7600 mass spectrometer (SCIEX, Framingham, MA, USA) equipped with an OptiFlow V source (SCIEX). The method employed on the Evosep One was 30SPD (samples per day), using a 44-min gradient with the EV1137 performance column (15 cm × 150 μm, 1.5 μm). The mass spectrometer operated in positive mode with a spray voltage set to 4500 V and relied on the sequential window acquisition of all theoretical mass spectra (SWATH) mode. The SWATH acquisition scheme included 85 variable-size windows covering a precursor mass range of 350–1250 *m/z* with an accumulation time of 0.02 s. All raw data from the ZenoTOF 7600 system (.wiff) were acquired using SCIEX OS software 3.3 and processed with data-independent acquisition by neural networks (DIA-NN 1.8.1) (Demichev, Messner et al. 2020) in a library-free mode. Spectra were compared against the *E.coli* K12 reference proteome database (https://www.uniprot.org/proteomes/UP000000625) or the *E. coli* O127:H6 (strain E2348/69 / EPEC) (https://www.uniprot.org/proteomes/UP000008205) with the following main settings: full tryptic digest allowing up to two missed cleavage sites, variable modifications including oxidized methionines and N-terminus acetylation, and fixed modification of carbamidomethylated cysteines. In addition, the "match-between-runs" option was enabled. The neural network classifier operated in single-pass mode, and protein inference was gene-based. Quantification was performed using robust LC (high precision). Cross-run normalization was retention time-dependent, and library generation used smart profiling. Statistical analysis was performed using an R script (available as a shinny app at https://analyst-suites.org/apps/dia-analyst) based on the protein-level data file. Contaminant proteins and reverse sequences were filtered out. The DIA abundance data was converted to $\log_2$ scale, samples were grouped by conditions and missing values were imputed using the "Perseus type" also named 'Missing not At Random' (MNAR) method),

which uses random draws from a left-shifted Gaussian distribution of 1.8 StDev (standard deviation) apart with a width of 0.3. For the differential expression analysis, protein-wise linear models combined with empirical Bayes statistics were used. The limma package from R Bioconductor was used to generate a list of differentially expressed proteins for each pair-wise comparison. A cutoff of the adjusted p-value of 0.05 (Benjamini-Hochberg method) along with a $|\log_2$ fold change$|$ of 1 has been applied to determine significantly regulated proteins in each pairwise comparison. Biomarkers proteins Log_2FC were cured from the published data set (Yu et al., 2020, O'Rourke et al. 2020). The gene ontology analysis of genes which exhibited at least 2-fold change ($p < 0.05$) was performed using David data base tools (Dennis Jr, Sherman et al. 2003). The Kyoto Encyclopedia of Genes and Genomes (KEGG) enrichment analysis was performed using ShinyGO 0.85.1 (https://bioinformatics.sdstate.edu/go), with the following settings FDR cut-off, 0.05; sort by genes; the total list of identified proteins was uploaded as "background".

Quantification and statistical analysis

All experiments were performed in minimum three replicates. Data were analyzed for significant differences using the statistical tests indicated in the figure legends or text, and included corrections for multiple testing when required. Statistical calculations and correlation analysis were performed using Prism or R Studio.

CRediT authorship contribution statement

Haitham Sedky: Conceptualization, Data curation, Formal analysis, Investigation, Visualization, Methodology, Writing – original draft. **Mohamed Belal Hamed:** Investigation, Methodology. **Kurt Vermeire:** Validation, Writing – review & editing. **Joost Schymkowitz:** Formal analysis, Validation, Writing – review & editing. **Spyridoula Karamanou:** Conceptualization, Validation, Funding acquisition, Resources, Project administration, Writing – review & editing, Supervision. **Anastassios Economou:** Conceptualization, Validation, Funding acquisition, Resources, Project administration, Supervision.

Declaration of competing interest

The authors declare that they have no known competing financial interests or personal relationships that could have appeared to influence the work reported in this paper.

Acknowledgements

We thank the Proteomics Leuven-Laboratory of Applied Mass Spectrometry (LAMaS) and the Genomics Core - UZ Leuven, in particular Khaled Mirzaei, for valuable help with proteomics and transcriptomics experiments; Joleen Masschelein from the Laboratory of Molecular Biotechnology of Plants and Microorganisms for WGS analysis; Patrick Chaltin, Arnaud Marchand, Vincent Pericolle and Matthias Versele from Cistim Leuven for providing the HSI#6 and HSI#11 compounds. Our research was supported by: KU Leuven (ZKD4582-C16/18/008 to AE and SK; #RUN/16/001 to AE); FWO/FNRS Excellence of Sciences (30550343/GOG0818N to AE), WoG/FWO (W002421N to AE) and FWO (G093519N; G009423N to AE). HS is supported by a scholarship provided by the Ministry of Higher Education and Scientific Research of the Arabic Republic of Egypt.

Supplementary materials

Supplementary material associated with this article can be found, in the online version, at doi:10.1016/j.crmicr.2026.100613.

Data availability

The authors declare that the data supporting the findings of this study are available within the paper and its Supplementary files. The mass spectrometry proteomics data have been deposited to the ProteomeXchange Consortium via the PRIDE partner repository with the dataset identifier PXD075099. Gene expression RNA-seq data, and whole genome sequencing data have been deposited at the NCBI Gene Expression Omnibus (GEO) accession number is GSE325691.

References

Abushaheen, M.A., et al., 2020. Antimicrobial resistance, mechanisms and its clinical significance. Disease-A-Month. 66 (6), 100971.
Ahmad, M., et al., 2025. The role of bacterial metabolism in antimicrobial resistance. Nat. Rev. Microbiol. 23 (7), 439–454.
Aita, S.E., et al., 2025. Proteomic insights into bacterial responses to antibiotics: a narrative review. Int. J. Mol. Sci. 26 (15).
Alam, A., et al., 2021. The role of ClpB in bacterial stress responses and virulence. Front Mol. Biosci. 8.
Aswal, M., et al., 2025. An integrated proteo-transcriptomics approach reveals novel drug targets against multidrug resistant *Escherichia coli*. Front Microbiol. 16–2025.
Bachar, A., et al., 2020. Point mutations in topoisomerase I alter the mutation spectrum in *E. coli* and impact the emergence of drug resistance genotypes. Nucleic Acids. Res. 48 (2), 761–769.
Barry, A.L., 1999. Methods for determining bactericidal activity of antimicrobial agents : approved guideline. NCCLS, M26-A 19, 21–27.
Bie, L., et al., 2023. Comparative analysis of transcriptomic response of *Escherichia coli K-12* MG1655 to nine representative classes of antibiotics. Microbiol. Spectr. 11 (2), e00317. -00323.
Bolger, A.M., et al., 2014. Trimmomatic: a flexible trimmer for Illumina sequence data. Bioinformatics 30 (15), 2114–2120.
Bollenbach, T., et al., 2009. Nonoptimal microbial response to antibiotics underlies suppressive drug interactions. Cell 139 (4), 707–718.
Boos, W., Shuman, H., 1998. Maltose/maltodextrin system of *Escherichia coli*: transport, metabolism, and regulation. Microbiol. Molecul. Biology. Rev. 62 (1), 204–229.
Borisov Vitaliy, B., Michael, I.Verkhovsky, 2015. Oxygen as acceptor. EcoSal Plus. 6 (2). https://doi.org/10.1128/ecosalplus.ESP-0012-2015.
Bury-Moné, S., et al., 2009. Global analysis of Extracytoplasmic stress signaling in *Escherichia coli*. PLoS Genet. 5 (9), e1000651.
Butler, M.S., et al., 2024. A Review of antibacterial candidates with new modes of action. ACS Infect. Dis. 10 (10), 3440–3474.
Chen, H., et al., 2023. Pseudomonas aeruginosa citrate synthase GltA influences antibiotic tolerance and the type iii secretion system through the stringent response. Microbiol. Spectr. 11 (1), e03239. -03222.
Dekker, N.H., et al., 2002. The mechanism of type IA topoisomerases. Proceed. Nation. Acad. Sci. 99 (19), 12126–12131.
Demichev, V., et al., 2020. DIA-NN: neural networks and interference correction enable deep proteome coverage in high throughput. Nat. Method. 17 (1), 41–44.
Dennis Jr, G., et al., 2003. DAVID: database for annotation, visualization, and integrated discovery. Genome Biol. 4 (9), R60.
Domínguez, Á., et al., 2017. Transcriptomics as a tool to discover new antibacterial targets. Biotechnol. Lett. 39 (6), 819–828.
Duitama, J., et al., 2014. An integrated framework for discovery and genotyping of genomic variants from high-throughput sequencing experiments. Nucleic Acid. Res. 42 (6), e44.
Elbaiomy, R.G., et al., 2025. Antibiotic resistance: a genetic and physiological perspective. MedComm 6 (11), e70447 (2020).
Espinoza, J.L., et al., 2021. Predicting antimicrobial mechanism-of-action from transcriptomes: a generalizable explainable artificial intelligence approach. PLoS Comput. Biol. 17 (3), e1008857.
Etchegaray, J.P., Inouye, M., 1999. CspA, CspB, and CspG, major cold shock proteins of *Escherichia coli*, are induced at low temperature under conditions that completely block protein synthesis. J. Bacteriol. 181 (6), 1827–1830.
French, S., et al., 2024. A platform for predicting mechanism of action based on bacterial transcriptional responses identifies an unusual DNA gyrase inhibitor. Cell Rep. 43 (4).
Gambushe, S.M., et al., 2026. Comparative genomics of diverse *Escherichia coli* O157:H7 strains to characterize plasmids, prophages, virulence and antimicrobial resistance genes. Plasmid 135, 102771.
Hafeezunnisa, M., Sen, R., 2020. The Rho-dependent transcription termination is involved in broad-spectrum antibiotic susceptibility in *Escherichia coli*. Front Microbiol. 11.
Hamed, M.B., et al., 2021. Effective small molecule Antibacterials from a novel anti-protein secretion screen. Microorganisms 9 (3).
Jackowski, S., et al., 2002. A missense mutation in the fabB (beta-ketoacyl-acyl carrier protein synthase I) gene confers tiolactomycin resistance to *Escherichia coli*. Antimicrob Agent. Chemother. 46 (5), 1246–1252.
Jensen, P.A., et al., 2017. Antibiotics disrupt coordination between transcriptional and phenotypic stress responses in pathogenic bacteria. Cell Rep. 20 (7), 1705–1716.

Jung, I.L., Kim, I.G., 2003. Transcription of ahpC, katG, and katE genes in *Escherichia coli* is regulated by polyamines: polyamine-deficient mutant sensitive to H2O2-induced oxidative damage. Biochem. Biophys. Res. Commun. 301 (4), 915–922.
Kim, D., et al., 2019. Graph-based genome alignment and genotyping with HISAT2 and HISAT-genotype. Nat. Biotechnol. 37 (8), 907–915.
Kitagawa, M., et al., 2005. Complete set of ORF clones of *Escherichia coli* ASKA library (A complete S et of *E. coli* K-12 ORF A rchive): unique resources for biological research. DNA Res. 12 (5), 291–299.
Kratz, J.C., Banerjee, S., 2024. Gene expression tradeoffs determine bacterial survival and adaptation to antibiotic stress. PRX Life. 2 (1), 013010.
Lang, M., et al., 2021. Sleeping ribosomes: bacterial signaling triggers RaiA mediated persistence to aminoglycosides. iScience 24 (10), 103128.
Larkins-Ford, J., Aldridge, B.B., 2023. Advances in the design of combination therapies for the treatment of tuberculosis. Expert Opin. Drug Discov. 18 (1), 83–97.
Larkins-Ford, J., et al., 2022. Design principles to assemble drug combinations for effective tuberculosis therapy using interpretable pairwise drug response measurements. Cell Rep. Med. 3 (9), 100737.
Li, X.-Z., et al., 2015. The Challenge of efflux-mediated antibiotic resistance in gram-negative bacteria. Clin. Microbiol. Rev. 28 (2), 337–418.
Li, Z., et al., 2020. The role of bacterial cell envelope structures in acid stress resistance in *E. coli*. Appl. Microbiol. Biotechnol. 104 (7), 2911–2921.
Liao, Y., et al., 2013. The Subread aligner: fast, accurate and scalable read mapping by seed-and-vote. Nucleic Acid. Res. 41 (10), e108.
Lobritz, M.A., et al., 2015. Antibiotic efficacy is linked to bacterial cellular respiration. Proc Natl. Acad. Sci. U S A 112 (27), 8173–8180.
Ma, S., et al., 2025. Mechanisms of *Staphylococcus aureus* antibiotics resistance revealed by adaptive laboratory evolution. Curr. Microbiol. 82 (1), 46.
Matuszewska, M., et al., 2005. The small heat shock protein IbpA of *Escherichia coli* cooperates with IbpB in stabilization of thermally aggregated proteins in a disaggregation competent state. J. Biologic. Chem. 280 (13), 12292–12298.
Miller, W.R., Arias, C.A., 2024. ESKAPE pathogens: antimicrobial resistance, epidemiology, clinical impact and therapeutics. Nat. Rev. Microbiol. 22 (10), 598–616.
Mo, C.Y., et al., 2018. Inhibitors of LexA Autoproteolysis and the bacterial SOS response discovered by an academic-industry partnership. ACS Infect. Dis. 4 (3), 349–359.
Morabito, A., et al., 2025. Algorithms and tools for data-driven omics integration to achieve multilayer biological insights: a narrative review. J. Transl. Med. 23 (1), 425.
Morales-Durán, N., et al., 2024. Unraveling resistance mechanisms in combination therapy: a comprehensive review of recent advances and future directions. Heliyon 10 (6), e27984.
Moskovitz, J., et al., 1995. *Escherichia coli* peptide methionine sulfoxide reductase gene: regulation of expression and role in protecting against oxidative damage. J. Bacteriol. 177 (3), 502–507.
Nunoshiba, T., et al., 1992. Two-stage control of an oxidative stress regulon: the *Escherichia coli* SoxR protein triggers redox-inducible expression of the soxS regulatory gene. J. Bacteriol. 174 (19), 6054–6060.
O'Rourke, A., et al., 2020. Mechanism-of-action classification of antibiotics by global transcriptome profiling. Antimicrob Agent.s Chemother. 64 (3).
Ocampo, P.S., et al., 2014. Antagonism between bacteriostatic and bactericidal antibiotics is prevalent. Antimicrob. Agent. Chemother. 58 (8), 4573–4582.
Palmer, A., Kishony, R., 2014. Opposing effects of target overexpression reveal drug mechanisms. Nat. Commun. 5, 4296.
Pettigrew, D.W., et al., 1988. *Escherichia coli* glycerol kinase. Cloning and sequencing of the glpK gene and the primary structure of the enzyme. J. Biologic. Chem. 263 (1), 135–139.
Piddock, L.J.V., et al., 2024. Challenges and opportunities with antibiotic discovery and exploratory research. ACS Infect. Dis. 10 (8), 2445–2447.
Poonawala, H., et al., 2024. Transcriptomic responses to antibiotic exposure in *Mycobacterium tuberculosis*. Antimicrob Agent. Chemother. 68 (5), e0118523.
Potamitou, A., et al., 2002. Expression of *Escherichia coli* glutaredoxin 2 is mainly regulated by ppGpp and sigmaS. J. Biol. Chem. 277 (20), 17775–17780.
Pulido, M.R., et al., 2016. Identifying targets for antibiotic development using omics technologies. Drug Discov. Today 21 (3), 465–472.
Rubio, T., et al., 2026. Combinations of colistin and bacteriocins prevent the selection of colistin resistance in Acinetobacter baumannii. Communication. Biol. 9 (1), 599.
S, A. (2010). "FastQC: a quality control tool for high throughput sequence data. Available online at:http://www.bioinformatics.babraham.ac.uk/projects/fastqc".
Schweizer, H., Boos, W., 1984. Characterization of the ugp region containing the genes for the phoB dependent sn-glycerol-3-phosphate transport system of *Escherichia coli*. Molecul. General Genetic. MGG 197 (1), 161–168.
Sedky, H., et al., 2026. A small molecule allosterically activates SecA dependent secretion. Communication. Biol. 9 (1), 368.
Senges, C.H.R., et al., 2020. Comparison of proteomic responses as global approach to antibiotic mechanism of action elucidation. Antimicrob. Agent. Chemother. 65 (1). https://doi.org/10.1128/aac.01373-01320.
Shah, S.N., et al., 2024. Antimicrobial resistance: an overview. Nanotechnol. Based Strategie. Combat. Antimicrob. Resist 1–44. M. Y. Wani, I. A. Wani and A. RaiSingapore, Springer Nature Singapore.
Sherry, N.L., et al., 2025. Genomics for antimicrobial resistance—progress and future directions. Antimicrob. Agent Chemother. 69 (5), e01082. -01024.
Tang, P.C., et al., 2024. Within-species variability of antibiotic interactions in gram-negative bacteria. mBio 15 (3), e0019624.
Thomas, J.G., Baneyx, F., 1998. Roles of the *Escherichia coli* small heat shock proteins IbpA and IbpB in thermal stress management: comparison with ClpA, ClpB, and HtpG In Vivo. J. Bacteriol. 180 (19), 5165–5172.
Torres-Sangiao, E., et al., 2022. Proteomic approaches to unravel mechanisms of antibiotic resistance and immune evasion of bacterial pathogens. Front Med (Lausanne) 9, 850374.
Tse-Dinh, Y.-C., 2008. Bacterial topoisomerase I as a target for discovery of antibacterial compounds. Nucleic Acids Res. 37 (3), 731–737.
Usongo, V., Drolet, M., 2014. Roles of type 1A topoisomerases in genome maintenance in *Escherichia coli*. PLoS Genet. 10 (8), e1004543.
Usui, M., et al., 2023. Intermittent antibiotic treatment of bacterial biofilms favors the rapid evolution of resistance. Commun. Biol. 6 (1), 275.
Vaisbourd, E., et al., 2025. Principles of bacteriostatic and bactericidal antibiotics at subinhibitory concentrations. mBio 16 (11), e02066. -02025.
Wang, C., et al., 2021. Molecular basis for substrate recognition by the bacterial nucleoside transporter NupG. J. Biol. Chem. 296, 100479.
Warrier, T., et al., 2022. Integrated genomics and chemical biology herald an era of sophisticated antibacterial discovery, from defining essential genes to target elucidation. Cell Chemic. Biol. 29 (5), 716–729.
Wecke, T., Mascher, T., 2011. Antibiotic research in the age of omics: from expression profiles to interspecies communication. J. Antimicrob. Chemother 66 (12), 2689–2704.
Wiegand, I., et al., 2008. Agar and broth dilution methods to determine the minimal inhibitory concentration (MIC) of antimicrobial substances. Nat. Protoc. 3 (2), 163–175.
Wood, T.K., 2009. Insights on *Escherichia coli* biofilm formation and inhibition from whole-transcriptome profiling. Environ. Microbiol. 11 (1), 1–15.
Xu, T., et al., 2026a. Identification of Rutaecarpine-Pyridinium quaternary ammonium conjugates exhibiting dual mechanisms of membrane-targeting and DNA Topo I inhibition as potent antimicrobials against methicillin-resistant staphylococcus aureus. J. Med. Chem. 69 (7), 8094–8114.
Xu, T., et al., 2026b. Overcoming methicillin-resistant *Staphylococcus aureus* infections by disrupting membrane integrity and inducing DNA degradation with a dual-mechanism fluorescent phenanthro[9,10-d]imidazole molecule. Research 9, 1242.
Yang, J., et al., 2015. Antimicrobial susceptibility and SOS-dependent increase in mutation frequency are impacted by *Escherichia coli* topoisomerase I C-terminal point mutation. Antimicrob Agent. Chemother 59 (10), 6195–6202.
Yousfi, M.M., et al., 1995. Metronidazole, omeprazole and clarithromycin: an effective combination therapy for *Helicobacter pylori* infection. Aliment Pharmacol. Ther. 9 (2), 209–212.
Yu, X.-Q., et al., 2025. Targeting efflux pumps prevents the multi-step evolution of high-level resistance to fluoroquinolone in *Pseudomonas aeruginosa*. Microbiol. Spectr. 13 (4), e02981. -02924.
Yu, Y., et al., 2020. Predictive Signatures of 19 antibiotic-induced *Escherichia coli* proteomes. ACS Infect. Dis. 6 (8), 2120–2129.
Zhang, Z., et al., 2022. Assessment of global health risk of antibiotic resistance genes. Nat. Commun. 13 (1), 1553.
Zhao, Q., et al., 2023. OmpA is involved in the early response of *Escherichia coli* to antibiotics as a hub outer membrane protein. Appl. Biochem. Microbiol. 59, 608–621.
Zhu, M., Dai, X., 2020. Bacterial stress defense: the crucial role of ribosome speed. Cell. Molecul. Life Sci. 77 (5), 853–858.